Improved efficiency of GaSb solar cells using an Al0.50Ga0.50As0.04Sb0.96 window layer

Stéphanie Parola, Alexandre Vauthelin, Julie Tournet, Joanna Kret, Joanna El Husseini, F. Martinez, Y. Rouillard, E. Tournié, Y. Cuminal

Improved efficiency of GaSb solar cells using an $Al_{0.50}Ga_{0.50}As_{0.04}Sb_{0.96}$ window layer

S. Parola,[a*] A. Vauthelin,[a] J. Tournet, [a] J. Kret, [a] J. El Husseini, [a] F. Martinez, [a] Y. Rouillard, [a] E. Tournié, [a] Y. Cuminal [a]

[a] IES, Univ. Montpellier, CNRS, F- 34000, Montpellier, France
* corresponding author: stephanie.parola@umontpellier.fr

Abstract

The increasing number of subcells in multi-junction structures imposes the use of narrow bandgaps for a full harvesting of the solar spectrum. In this context, gallium antimonide (GaSb) and its lattice-matched alloys offer a great potential. To date, GaSb-based multi-junction solar cells exhibit experimental results below theoretical expectations, due to a limiting GaSb subcell. In this paper, a new design of GaSb cells comprising an $Al_{0.50}Ga_{0.50}As_{0.04}Sb_{0.96}$ window layer is studied. With this design, an excellent conversion efficiency of 7.2% is achieved under 1 sun (AM1.5G) illumination. This performance is attributed to a significant improvement in short-circuit current.

Keywords

GaSb; AlGaAsSb; window layer; III-V multi-junction solar cells; antimonide alloys.

1. Introduction

Gallium antimonide (GaSb) had been first introduced into the photovoltaic field as a subcell of mechanically stacked GaAs/GaSb tandem cells [1]. It was then widely studied as a single cell or as part of a lattice-matched tandem cell (GaSb/GaInAsSb) for thermophotovoltaic applications [2]–[4]. Recently, GaSb has attracted a lot of scientific attention within the domain of multi-junction solar cells thanks to the large availability of alloys (AlGaAsSb, AlInAsSb and GaInAsSb) lattice-matched to GaSb. These alloys offer a wide coverage of bandgap energies, which is essential for an efficient solar spectrum harvesting, mainly at longer wavelengths [5], [6]. Also, recent progress in the fabrication process (metamorphic growth, wafer bonding and transfer printing) has led to an easier implementation of these materials into multi-junction structures [7]–[10]. However, latest results on GaSb-based multi-junction solar cells indicate the limiting performance of this subcell. More specifically, GaSb subcells tend to deliver low values of J_{sc} – a behavior attributed to front-surface recombination losses [7], [11]. In order to minimize these losses in a 2-terminal multi-junction cell, the design of the GaSb cell has to be optimized by improving the window layer. The use of various window layers, such as $Al_{0.20}Ga_{0.80}Sb$ [7], $Al_{0.30}Ga_{0.70}Sb$ [9] or $Al_{0.20}Ga_{0.80}As_{0.02}Sb_{0.98}$ [3] has already been reported in the literature but has not entirely overcome this issue. This paper reports on the design and performance of a GaSb single-junction solar cell grown by molecular-beam epitaxy (MBE), comprising an $Al_{0.50}Ga_{0.50}As_{0.04}Sb_{0.96}$ window layer. Based on the experimental results, the potential of the GaSb cell as subcell of 4- and 5-junction solar cells is assessed.

2. Experimental details

The epitaxial layers were grown by MBE on epi-ready n-type GaSb (001) substrate in a Varian GEN II reactor. The substrate was deoxidized at 550 °C under Sb flux. The substrate temperature was estimated by cross-calibrated thermocouple and pyrometer measurements. This temperature was also confirmed by the GaSb (001) – (2x5) to (1x3) surface reconstruction switch at 415 °C under an Sb flux of 1 ML/s [12]. After 20 min of deoxidation, a 200 nm n-doped GaSb buffer layer was grown at 500 °C. The solar cell was then grown at the same temperature. Its structure, depicted in Fig. 1, comprises a 25 nm n-doped $Al_{0.50}Ga_{0.50}As_{0.04}Sb_{0.96}$ back surface field layer (BSF), a 3 µm n-doped GaSb base, a 100 nm p-doped GaSb emitter, a 10 nm p-doped $Al_{0.50}Ga_{0.50}As_{0.04}Sb_{0.96}$ window layer and a 10 nm p-doped GaSb cap layer to prevent oxidation of the Al-rich window layer. For the sake of simplicity, the $Al_{0.50}Ga_{0.50}As_{0.04}Sb_{0.96}$ composition will be referred to as AlGaAsSb in the remainder of the text. Te and Be were used for n-type and p-type doping, respectively. The corresponding

doping levels are indicated in Fig. 1. The base and emitter were grown at 0.8 ML/s, the BSF and window layers at 1 ML/s, and the buffer and cap layers at 0.5 ML/s. During growth, *in-situ* reflection high electron energy diffraction (RHEED) monitoring exhibited streaky patterns, indicating smooth epitaxy. After growth, the sample was analyzed by high-resolution X-ray diffraction (HRXRD). The omega-2 theta scan is shown in Fig. 2 and confirms that the quaternary alloy is lattice-matched to GaSb. Fitting to the experimental curve with the Epitaxy and Smoothfit software (PANalytical) allowed to determine an arsenic content of 0.04 in the quaternary layer.
A 300 nm-thick AuGeNi alloy was deposited by sputtering on the rear surface to serve as a back contact. A rapid thermal annealing (RTA) was subsequently performed at 275 °C during 1 min, in order to reach a specific contact resistivity of 10^{-4} Ω.cm^2. This latter value was extracted from circular transmission line model (CTLM) measurements. Then, after the UV-lithography of the metallic grid pattern, the Ti/Pt/Au (20 nm / 30 nm / 150 nm) front contact was deposited by e-beam evaporation. The contact was annealed by RTA at 250°C during 1 min to attain a specific contact resistivity of $3x10^{-7}$ Ω.cm^2 (extracted from CTLM). The front contact grid is illustrated in Fig. 1 (b) and presents an 11 % shading factor (area covered by metal to total area ratio).
A chemical solution of $HCl:H_2O_2:H_2O$ (1:1:1) was used for the wet etching of the mesas in order to delimit the surface of the cell (6.1 x 6.7 mm²). Last, a 175 nm-thick SiO_2 antireflection coating (ARC) was deposited on the front surface by sputtering.

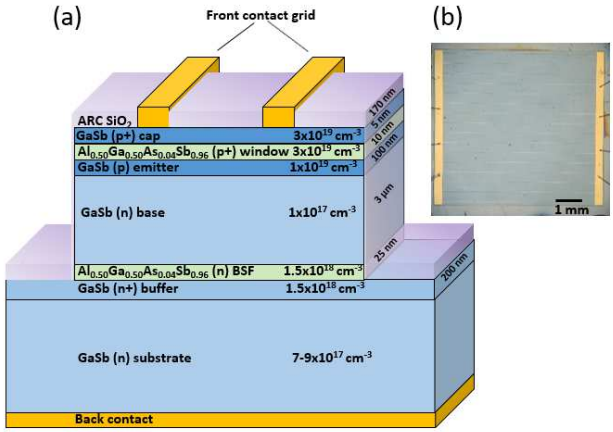

Fig. 1. (a) Schematic structure and (b) microscope image of the fabricated GaSb solar cell.

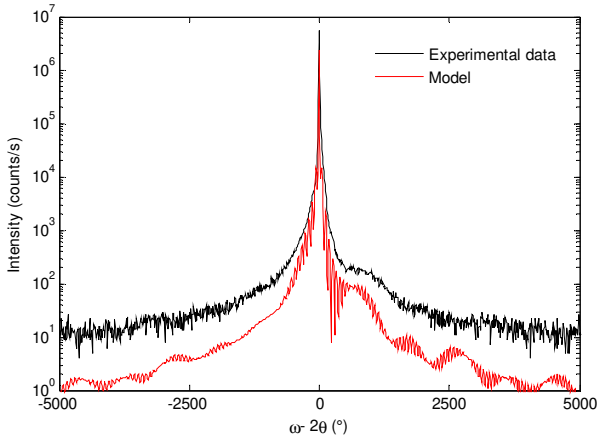

Fig. 2. HRXRD omega-2 theta scan of the epitaxial structure and its simulation with the Epitaxy and Smoothfit software (PANalytical). The simulated curve has been vertically shifted for the sake of clarity.

The spectral response was measured with a custom-built setup composed of a Xenon lamp, a monochromator equipped with two diffraction gratings, a filter wheel to remove the higher diffraction orders of radiation, and a lock-in amplifier. The measurements were calibrated with Si and Ge photodiodes (Thorlabs FDS100-CAL and FDG03-CAL, respectively) to cover the whole wavelength range of interest. The reflectance curve was measured with a Jasco V-670 UV-VIS-NIR spectrophotometer.
The current density-voltage (J-V) curves were measured with a Keithley 2400 sourcemeter. During measurement, the cell temperature was regulated at 25 °C using a Peltier element. The J-V characteristics were acquired under dark and 1-sun illumination conditions. The constant irradiation was provided by a Newport ORIEL Sol 3A solar simulator (Class AAA) composed of a Xenon lamp and an AM1.5G spectral correction

filter. The light intensity was calibrated at the equivalent of 1-sun AM1.5G solar spectrum over the 350-1800 nm wavelength range by adjusting the spectral mismatch factor using two reference cells (Si and Ge). It was also verified that the J_{sc} calculated from spectral response measurement was in agreement with the measured J_{sc}. It should be noted that the measured J_{sc} takes into account the busbar shading.

3. Modeling

Numerical simulations were performed to compute the reflectance (R), external quantum efficiency (EQE), internal quantum efficiency (IQE) and J-V curves of the device under dark and illumination conditions. For this purpose, an in-house MATLAB code solving the fully-coupled semiconductor (Poisson and continuity) equations in one dimension was developed. A special attention was paid to the heterojunction modeling (especially the heterojunctions induced by the window layer and the BSF) by using double-valued mesh points for the quasi-Fermi levels at hetero interfaces [13]. In addition to bulk recombination, interface Shockley-Read-Hall (SRH) recombination involving surface recombination velocities (SRV) for electrons and holes was implemented. The optical generation was calculated using a transfer-matrix-based method, involving optical properties (n, k) taken either from literature (GaSb [14]) or from experimental ellipsometry data (SiO_2 and AlGaAsSb [5]).
An impurity-dependent mobility expression was used for GaSb [15]. The other material parameters (of GaSb and AlGaAsSb) used for the simulations are summarized in Table I. More details on the estimation of the physical parameters of the quaternary alloy used for simulations are reported in [5]. The radiative and Auger recombination parameters of GaSb were used for AlGaAsSb due to a lack of experimental data. Electron and hole SRH lifetimes were estimated at 1 ns for the AlGaAsSb alloy, which is a typical value for III-V materials.

4. Results and discussion

Fig. 3 presents the dark and 1-sun J-V measurements of the GaSb solar cell. The figures of merit of the 1-sun experimental curve are summarized in Table II. The cell exhibits a 1-sun efficiency of 7.2 % which is, to the best of our knowledge, the highest published value for a GaSb solar cell so far. This excellent performance is mainly due to the presence of the AlGaAsSb window layer that allows to reach a J_{sc} of 38.8 mA/cm^2, *i.e.* 66 % of the Shockley-Queisser radiative limit [16].
Results of the numerical simulations are shown in Fig. 3 (J-V curves) and Fig. 4 (R, EQE and IQE curves). A comparison between experimental and simulated 1-sun figures of merit is provided in Table II. SRH lifetime of minority carriers, SRV, shunt and series resistances were adjusted to provide the best fit to the experimental curves for both J-V and EQE measurements. The material parameters used for these simulations are given in Table I. The bulk SRH lifetime in the base ($\tau_{SRH,h}$) was set to 50 ns (instead of the typical value 600 ns [15]). The bulk lifetime in the emitter ($\tau_{SRH,e}$) affects neither the J-V nor the EQE curves and was therefore fixed at its typical value – 10 ns. The value of SRV at each AlGaAsSb/GaSb interface of the device is assumed to be the same for electrons and holes (S_n=S_p=S) and estimated at 10^4 cm/s. This value is of the same order of magnitude as previously reported SRV at AlGaAsSb/GaSb interface [3], [7]. The values of the shunt and series resistances (R_{shunt} and R_s) derived from the dark J-V curve are approximately 2850 Ω.cm^2 and 3x10^{-2} Ω.cm^2, respectively. Both values are comparable to previously published results [9], [10].
The difference in FF between the measured and the modeled data is usually attributed to the series resistance losses. A more accurate estimation of the FF would require the use of a 3D distributed model taking into account all series resistance components [17].

Table I. Material parameters used for simulations.

	Electron affinity	Bandgap	Relative permittivity	Effective mass		Mobility	Recombination parameters		
Material	χ (eV)	E_g (eV)	ε_r	m_e^*/m_0	m_h^*/m_0	μ_n μ_p (cm^2/V.s)	C_n C_p (cm^6/s)	B (cm^3/s)	$\tau_{SRH,e}$ $\tau_{SRH,h}$ (ns)
GaSb	4.06	0.726	15.7	0.039	0.800	[15]	5x10^{-30}	8.5x10^{-11}	{10 , 50}
$Al_{0.50}Ga_{0.50}As_{0.04}Sb_{0.96}$	3.83	1.35	13.8	0.077	0.883	{200, 530}	5x10^{-30}	8.5x10^{-11}	{1 , 1}

Table II. 1-sun figures of merit of the experimental and simulated J-V curves.

	J_{sc} (mA/cm^2)	V_{oc} (mV)	FF (%)	η (%)
Measured	38.8	312.2	59.6	7.2
Modeled	38.8	313.3	65.1	7.9

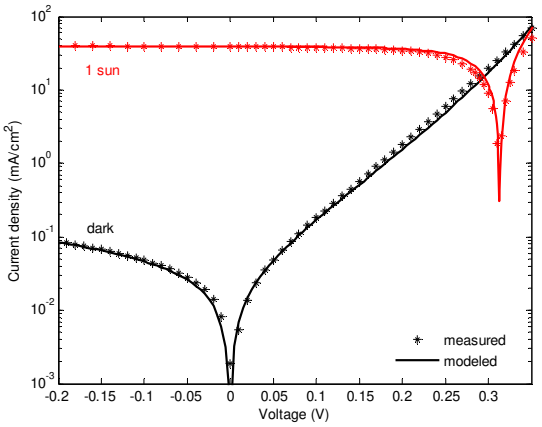

Fig. 3. Measured (symbols) and modeled (solid lines) dark and 1-sun J-V characteristics (respectively in black and in red) of the GaSb cell comprising AlGaAsSb window and BSF layers.

The IQE values (Fig. 4), calculated using measured reflectance data, exceed 90 % over the [650 - 1530] nm wavelength range. This result demonstrates an efficient carrier collection over a large fraction of the spectral range of interest. This observation is corroborated by the estimation of a SRH minority carrier lifetime in the base corresponding to a diffusion length of about 10 µm. The difference between the EQE and IQE curves could be reduced by using a more efficient ARC.

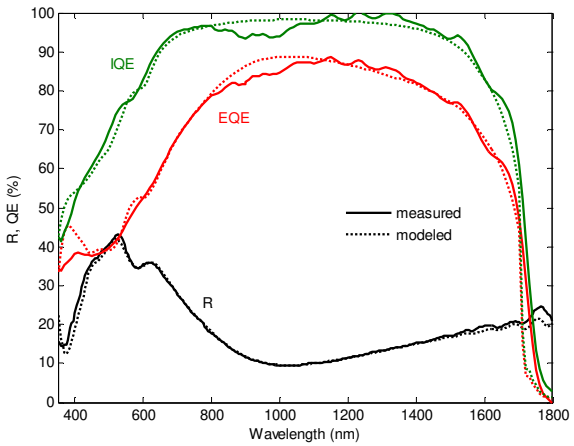

Fig. 4. Measured (solid lines) and modeled (dotted lines) relectivity, EQE and IQE curves of the GaSb cell comprising AlGaAsSb window and BSF layers.

Fig. 5 (a) and (b) present numerical simulations and show the impact of the SRH bulk recombination and the SRV on the dark J-V and IQE curves for the studied cell structure. Two different SRH hole lifetimes – 50 ns and 600 ns are taken into consideration. They correspond respectively to the base lifetime adjusted to fit the experimental data and the standard value of SRH bulk lifetime. For SRV, two values are also investigated: 10^3 cm/s – typical for a standard interface obtained by MBE growth – and 10^6 cm/s – a value corresponding to a poor-quality interface. A particular SRV is set at each AlGaAsSb/GaSb interface in the device. Both bulk and surface recombination affect the IQE in a similar way, decreasing its value at long wavelengths. However, at short wavelengths, the IQE is not impacted by a change in SRV. This is due to the thin emitter layer where the neutral region's width is likely smaller than the diffusion length of the electrons. A more pronounced impact of the above-mentioned recombination parameters can be noted on the dark J-V curve. Poorer SRH bulk lifetimes induce an up-shift of the entire curve while changes in SRV only affect the part of the curve where the diffusion

phenomena dominate. It can also be noted that the impact of the SRV is more significant for higher SRH bulk lifetimes. The dark J-V curve thus allows to dissociate the bulk and surface recombination effects.

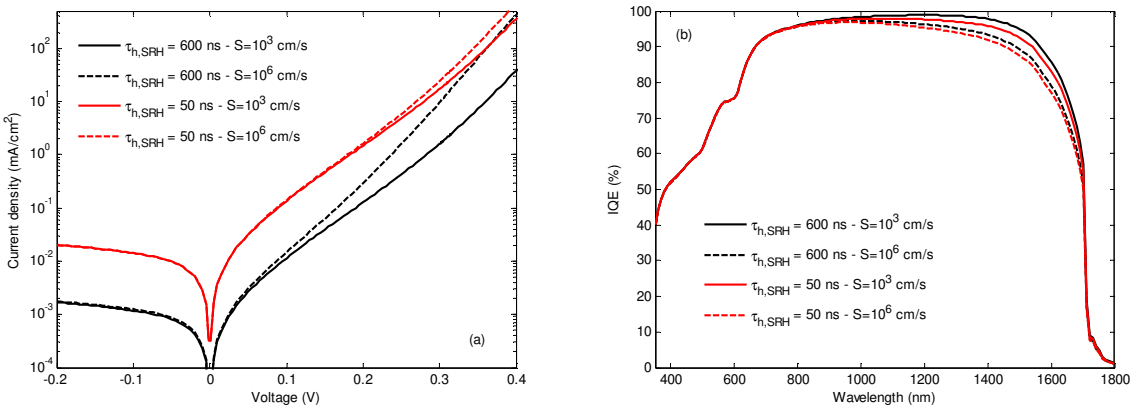

Fig. 5. Impact of the SRV at AlGaAsSb/GaSb interfaces and the SRH bulk lifetime on the dark J-V curve (a) and on the IQE curve (b).

In a 2-terminal multi-junction solar cell where lateral transport does not occur in the GaSb subcell, the window layer should exhibit the highest transparency and induce the largest potential barrier (on the minority carrier band) possible. A different set of numerical simulations was carried out in order to further investigate the $Al_xGa_{1-x}As_ySb_{1-y}$ window layer design. Fig. 6 (a) and (b) show the impact of the thickness and composition of the window layer on the J-V and IQE curves. Two distinct alloy compositions (x_{Al}=0.2 and 0.5) as well as two different window thicknesses (10 and 25 nm) were investigated. Higher Al contents of the quaternary alloy were not studied due to the fast oxidation of Al-rich materials. For these simulations, the SRV at the AlGaAsSb/GaSb interfaces were considered to not depend on the quaternary alloy composition (S is set to 10^4 cm/s, the value fitted to experimental data). It is important to note that the composition of the quaternary alloy allows to tune its bandgap by varying the Al content (x_{Al}) with the As content (y_{As}) being adjusted to ensure lattice matching to GaSb. The dependence on composition of the bandgap of these lattice-matched alloys has been modeled in [18]. The $Al_{0.20}Ga_{0.80}As_{0.02}Sb_{0.98}$ alloy exhibits a direct bandgap of 0.98 eV whereas $Al_{0.50}Ga_{0.50}As_{0.04}Sb_{0.96}$ alloy has an indirect bandgap of 1.35 eV. A window layer composed of an indirect and larger bandgap material results in a higher transparency as it can be observed in Fig. 6. Also, it seems that, regardless of the variations in the alloy composition, the increasing thickness leads to the reduction of the IQE values for short wavelengths as the absorption of this layer increases. The thickness and composition of the window layer do not affect the J-V curves, as shown in Fig. 6 (a).

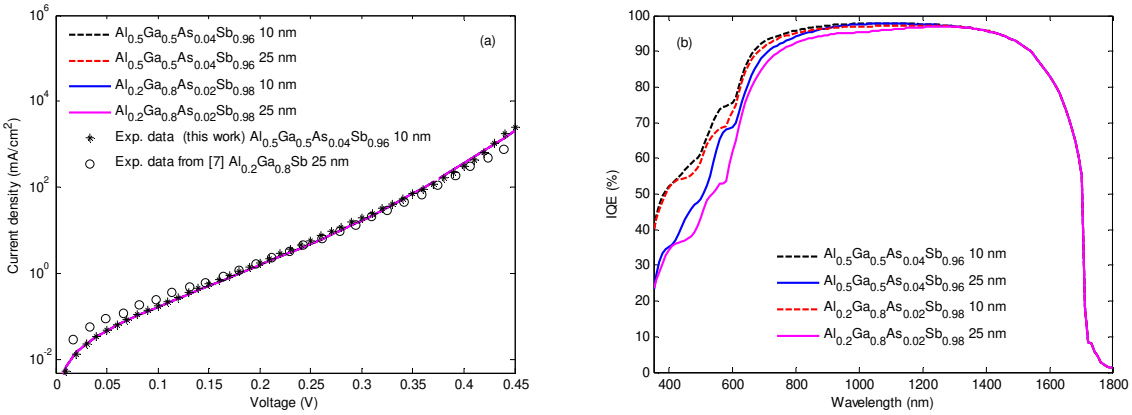

Fig. 6. Impact of the thickness and the composition of the window layer on the dark J-V curve (a) and on the IQE curve (b). All simulated curves on Fig. 6 (a) are overlaid. Experimental J-V curves (this work and from [7]) are also shown for comparison on Fig. 6 (a).

In Fig. 7, the studied cell design is compared to other designs reported in the literature: an $Al_{0.20}Ga_{0.80}Sb$ window layer (25 nm) on a GaSb p-on-n junction [7], an $Al_{0.30}Ga_{0.70}Sb$ window layer (30 nm) on a GaSb n-i-p junction [9], an $Al_{0.20}Ga_{0.80}As_{0.02}Sb_{0.98}$ window layer (50 nm) on a GaSb n-on-p junction [3] and a GaSb n-on-p junction without any window layer [19]. The $Al_{0.50}Ga_{0.50}As_{0.04}Sb_{0.96}$ layer allows to achieve higher IQE values over the [350 – 1600] nm wavelength range. The enhancement of the IQE values mainly occurs for wavelengths shorter than 700 nm and is attributed to a higher transparency of the $Al_{0.50}Ga_{0.50}As_{0.04}Sb_{0.96}$ window layer. A window

layer thicker than 10 nm (such as the ones reported in the literature) is not required to prevent the diffusion of the minority carriers (electrons) to the front surface.
On the other hand, for wavelengths longer than 1600 nm, the studied cell exhibits IQE values similar to other results from the literature with the exception of the better performing cell reported in [19]. It therefore suggests that the $Al_{0.50}Ga_{0.50}As_{0.04}Sb_{0.96}$ BSF does not improve the rear surface carrier collection. Further investigation on more efficient BSF, allowing to improve the collection of low photon energies – a crucial parameter for multi-junction applications – will be addressed in future works.

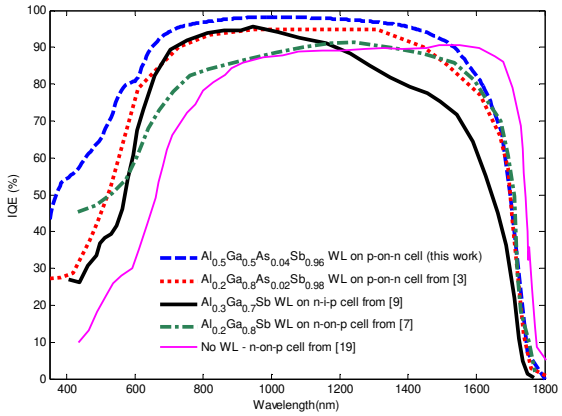

Fig. 7. Impact of various window layers (WL) on the IQE of GaSb cells. The IQE of the studied cell is compared to data from the litterature [3], [7], [9], [19].

Fig. 6 (a) also presents also the comparison of the experimental dark J-V curves of our device to the GaSb subcell studied in [7]. Clearly, both characteristics are very similar. This similarity experimentally demonstrates that the dark J-V curve does not depend on the window layer thickness and composition. As a consequence, the V_{oc} value obtained in this work only results from the increase in J_{sc} as the dark J-V curve does not change (in the approximation of the superposition principle).

In the context of multi-junction solar cells, GaSb has already been studied as part of 4- and 5-junction cells with GaInP/GaAs/GaInAs//GaSb [11] and InGaP/GaAs/InGaAsN//GaSb/InGaAsSb [7] architectures. In both cases, the GaSb subcell provided a limiting J_{sc} compared to the other subcells.
From detailed balance calculations [16], the target J_{sc} values required to satisfy the current-matching condition for the aforementioned 4- and 5-junction cells are respectively 13.5 and 12.3 mA/cm^2 (Table III). Therefore, the potential of the two GaSb designs exhibiting the best IQE values in Fig. 7 (*i.e.* the one studied in this work and the one presented in [19]) is assessed for multi-junction applications. For this purpose, it is necessary to estimate the J_{sc} they would deliver in such structures. The J_{sc} is calculated from the IQE curve (no reflection is assumed) and a filtered AM1.5D spectrum. The AM1.5D spectrum is filtered for energies higher than the upper subcell bandgap, *i.e.* 1.08 eV and 1.0 eV, which correspond to GaInAs and InGaAsN subcells of above-mentioned 4- and 5-junction solar cells. The calculated J_{sc} values are summarized in Table III. For a 4-junction application, the GaSb cell investigated in this work and the one reported in [19] would deliver 13.5 mA/cm^2 and 12.8 mA/cm^2, respectively. Therefore, the studied GaSb cell would reach the expected J_{sc} value in a 4-junction structure. In the case of the 5-junction cell however, the J_{sc} values of both GaSb cell designs still remain too low to meet the expectations.

Table III. Calculated J_{sc} values of GaSb subcells as a part of a 4- and 5-junction solar cells. The target values, calculated from the detailed balance model, are given for comparison.

J_{sc} of the GaSb subcell	4-junction cell	5-junction cell
Studied cell in this work	13.5 mA/cm^2	9.9 mA/cm^2
Calculated from Tang *et al.* [19]	12.8 mA/cm^2	10.0 mA/cm^2
Target values	13.5 mA/cm^2	12.3 mA/cm^2

5. Conclusion

We have reported experimental results on a p-on-n GaSb solar cell comprising an $Al_{0.50}Ga_{0.50}As_{0.04}Sb_{0.96}$ window layer. We have demonstrated that the use of this specific window layer improves substantially the short-circuit current. This leads to a conversion efficiency of 7.2 % under AM1.5G illumination, which is currently the highest published value for GaSb cells. We have shown that the studied cell design is a good candidate as a subcell in a 2-terminal 4-junction structure. This result paves the way to the development of all lattice-matched multi-junction cells on GaSb for concentrated photovoltaic systems.

Acknowledgments

This work was partly supported by the French program on « Investments for the future » managed by the National Agency for Research under contracts ANR-10-LABX-22-01-SOLSTICE and ANR-11-EQPX-0016 (Equipex EXTRA) and the H2020 program through MSCA ITN PROMIS (GA 641899).

References

[1] L. M. Fraas *et al.*, "Over 35-Percent Efficient GaAs / GaSb Tandem Solar," *IEEE Trans. Electron Devices*, vol. 37, no. 2, pp. 443–449, 1990.

[2] V. M. Andreev *et al.*, "Tandem GaSb/lnGaAsSb Thermophotovoltaic Cells," *Proc. 26th IEEE PV Spec. Conf.*, pp. 935–938, 1997.

[3] A. W. Bett and O. V. Sulima, "GaSb photovoltaic cells for applications in TPV generators," *Semicond. Sci. Technol.*, vol. 18, no. 5, pp. S184–S190, 2003.

[4] A. Datas and A. Martí, "Thermophotovoltaic energy in space applications : Review and future potential," *Sol. Energy Mater. Sol. Cells*, vol. 161, pp. 285–296, 2017.

[5] S. Parola *et al.*, "Investigation of antimonide-based semiconductors for high- efficiency multi-junction solar cells," *Proc. IEEE 7th World Conf. Photovolt. Energy Convers.*, 2018.

[6] M. P. Lumb *et al.*, "Towards the Ultimate Multi-Junction Solar Cell Using Transfer Printing," *Proc. 43rd IEEE PV Spec. Conf.*, pp. 40–45, 2016.

[7] M. P. Lumb *et al.*, "GaSb-Based Solar Cells for Full Solar Spectrum Energy Harvesting," *Adv. Energy Mater.*, vol. 1700345, pp. 1–9, 2017.

[8] A. Mansoori *et al.*, "Reducing threading dislocation density in GaSb photovoltaic devices on GaAs by using AlSb dislocation filtering layers," *Sol. Energy Mater. Sol. Cells*, vol. 185, pp. 21–27, 2018.

[9] G. T. Nelson *et al.*, "GaSb solar cells grown on GaAs via interfacial misfit arrays for use in the III-Sb multi-junction cell," *Appl. Phys. Lett.*, vol. 111, no. 231104, pp. 0–5, 2017.

[10] J. Tournet *et al.*, "GaSb Solar Cells for Multi-junction Solar Cell Integration on Si substrates," *Sol. Energy Mater. Sol. Cells*, vol. 191, pp. 444–450, 2019.

[11] F. Dimroth *et al.*, "Four-Junction Wafer-Bonded Concentrator," *IEEE J. Photovoltaics*, vol. 6, no. 1, pp. 343–349, 2016.

[12] A. S. Bracker, M. J. Yang, B. R. Bennett, J. C. Culbertson, and W. J. Moore, "Surface reconstruction phase diagrams for InAs, AlSb, and GaSb," *J. Cryst. Growth*, vol. 220, no. 4, pp. 384–392, 2000.

[13] M. Grupen, K. Hess, and G. H. Song, "Simulation of Transport over Heterojunctions," *Simul. Semicond. Devices Process*, vol. 4, pp. 303–311, 1991.

[14] S. Adachi, "Optical dispersion relations for GaP, GaAs, GaSb, InP, InAs, InSb, AlxGa1−xAs, and In1−xGaxAsyP1−y," *J. Appl. Phys.*, vol. 66, no. 12, pp. 6030–6040, 1989.

[15] L. Tang, L. M. Fraas, Z. Liu, C. Xu, and X. Chen, "Performance Improvement of the GaSb Thermophotovoltaic Cells With n-Type Emitters," *IEEE Trans. Electron Devices*, vol. 62, no. 9, pp. 2809–2815, 2015.

[16] W. Shockley and H. J. Queisser, "Detailed Balance Limit of Efficiency of pn Junction Solar Cells," *J. Appl. Phys.*, vol. 32, no. 1961, pp. 510–519, 1961.

[17] B. Galiana, C. Algora, and I. Rey-Stolle, "Comparison of 1D and 3D analysis of the front contact influence on GaAs concentrator solar cell performance," *Sol. Energy Mater. Sol. Cells*, vol. 90, pp. 2589–2604, 2006.

[18] S. Adachi, "Band gaps and refractive indices of AlGaAsSb, GaInAsSb, and InPAsSb: Key properties for a variety of the 2-4-μm optoelectronic device applications," *J. Appl. Phys.*, vol. 61, no. 10, pp. 4869–4876, 1987.

[19] L. Tang, L. M. Fraas, Z. Liu, Y. Zhang, H. Duan, and C. Xu, "N-type vapor diffusion for the fabrication of GaSb thermophotovoltaic cells to increase the quantum efficiency in the long wavelength range," *Sol. Energy Mater. Sol. Cells*, vol. 194, pp. 137–141, 2019.